Journal of Magnetic Resonance **144,** 6–12 (2000)
doi:10.1006/jmre.1999.2009, available online at http://www.idealibrary.com on IDEAL®

t_1 Noise and Sensitivity in Pulsed Field Gradient Experiments

Guoxing Lin,[1] Xinli Liao, Donghai Lin, Shaokuan Zheng, Zhong Chen, and Qinyi Wu

Department of Chemistry, Xiamen University, Xiamen 361005, People's Republic of China

Received January 22, 1999; revised September 16, 1999

In this paper, a calculation routine based on product operator formalism and coherence pathway is presented, which describes t_1 noise and sensitivity in pulsed field gradient experiments. Several examples including the absolute value mode pulsed field gradient COSY, MQF-COSY, MQC, HMQC, and NOESY sequences are investigated to study the t_1 noise stemming from the phase errors of radiofrequency (RF) pulses and the sensitivity affected by RF pulse rotation angles. Our theoretical results indicate that the t_1 noises in P-type COSY, multiple-quantum-filtered (MQF)-COSY, and multiple-quantum coherence (MQC) are lower than those in the N-type corresponding experiments, while in HMQC and NOESY there is no difference in t_1 noise effects between P-type and N-type spectra. Meanwhile, from the calculations, we obtained the optimized RF pulse rotation angles in those sequences. In MQF-COSY, an increase in sensitivity of about $4(\cos^2\theta \sin^{q-1}2\theta)^2 - 1$ (θ = arc cot $\sqrt{2/(q-1)+1}$)can be achieved by using the optimized angles. In MQC, the increase is $2\cos^2\theta \sin^{q-1}2\theta - 1$ (θ = arc cot $\sqrt{2/(q-1)+1}$). MQF-COSY experiments are also carried out to support our corresponding theoretical results. © 2000 Academic Press

Key Words: **NMR; PFG; t_1 noise; sensitivity; RF pulse.**

I. INTRODUCTION

The applications of NMR spectroscopy are often limited by the low concentration of molecules of interest in situations such as *in vivo* spectroscopy (*1*). As a result, any means of increasing the signal strength or decreasing noise is important. The signal strength and t_1 noise are closely related to the RF (radiofrequency) pulses of sequence. The arbitrary phase errors of RF pulses caused by instrumental irreproducibilities will result in t_1 noise. Recently the ratio of t_1 noise in P-type to that in N-type spectra has been evaluated in the PFG (pulsed field gradient) COSY experiment (*2, 3*). In addition, the rotation angles of RF pulses will determine the amplitude of the observable signal. For example, RF pulse angles other than 90° have been used to detect double-quantum frequencies (*4, 5*).

In this paper, we use a convenient calculation routine to describe the effects of RF pulses on the phase error and amplitude of the FID signal. Based on the product operator formalism (*6*), in combination with the coherence pathway, we calculated the absolute value mode PFG COSY, MQF-COSY (multiple-quantum-filtered COSY), MQC (multiple-quantum coherence), HMQC, and NOESY experiments (*7, 8*). From the calculations, the t_1 noise levels are obtained straightforwardly according to Parseval's theorem, and the optimized RF pulse rotation angles in those sequences are also determined.

II. THEORY

The sequences for the absolute value mode P-type and N-type pulsed field gradient COSY, MQF-COSY, MQC, HMQC, and NOESY experiments are shown in Fig. 1. In Fig. 1, α, β, and γ are the rotation angles of RF pulses, and ϵ_i is the phase error of the RF pulse caused by instrumental instabilities. In the calculations, we give out only those terms that can survive the coherence transfer pathway and consider only the effects of the RF pulses on the evolution of spin I_i. Because chemical shift and scalar coupling are mainly responsible for the precessing frequencies of the signal in P-type and N-type experiments, and the PFG pulses are mainly used to select out the desired coherence pathway in P-type and N-type experiments, we neglect those effects in the calculations.

A. Phase Error and Intensity of FID Signal

Consider the transformation of density operators under RF pulse (*6*)

$$I_z \xrightarrow{\theta(I_x\cos\epsilon + I_y\sin\epsilon)} I_z\cos\theta + \frac{i}{2}[I^+\exp(-i\epsilon) - I^-\exp(i\epsilon)]\sin\theta \qquad [1]$$

$$I^\pm \xrightarrow{\theta(I_x\cos\epsilon + I_y\sin\epsilon)} I^\pm\cos^2\frac{\theta}{2} + I^\mp\sin^2\frac{\theta}{2}\exp(\pm i2\epsilon) \pm iI_z\sin\theta\exp(\pm i\epsilon), \qquad [2]$$

where θ is the rotation angle of the RF pulse, and ϵ is the small phase error of the RF pulse caused by the instrumental irre-

[1] To whom correspondence should be addressed. E-mail: Lingx@jingxian.xmu.edu.cn.

1090-7807/00 $35.00

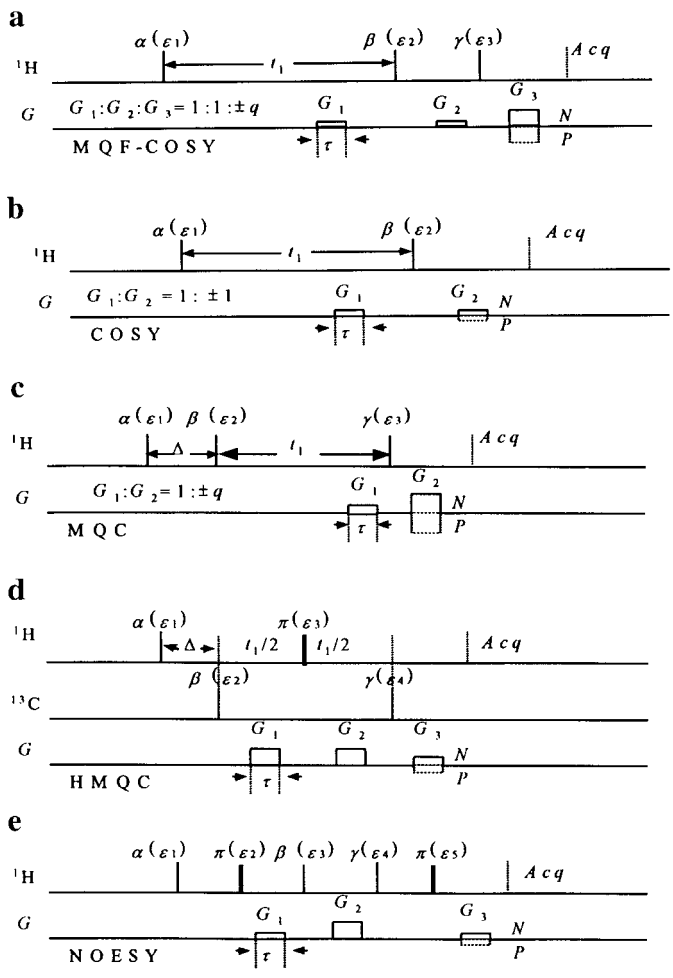

FIG. 1. Pulse sequences for absolute value mode pulsed field gradient (a) MQF-COSY, (b) COSY, (c) MQC, (d) HMQC, and (e) NOESY. α, β, and γ are the rotation angles of the RF pulses, and ϵ_i is the phase error of the RF pulse caused by instrumental instabilities.

producibility. In Eqs. [1] and [2], the density operators on the right-hand side are modulated by θ and ϵ in amplitude and phase, respectively. The transformation coefficients are different in different coherence transfer pathways. For example, in pathways $I^+ \rightarrow I^-$ and $I^- \rightarrow I^-$, the changes of signal are proportional to $\sin^2(\theta/2)\exp(+i2\epsilon)$ and $\cos^2(\theta/2)$, respectively. So in the experiments with different coherence transfer pathways and different RF pulse angles, the phase errors and the amplitudes of the FID signal will be different. In the following, we follow the example of absolute value mode PFG MQF-COSY (Fig. 1).

In the N-type PFG MQF-COSY, the coherence pathway is $0 \rightarrow +1 \rightarrow +q \rightarrow -1$, in which q is the order of coherence. We assume that a spin system with q weakly coupled spins is initially at equilibrium state. For simplicity, we consider only the density operator evolution of spin I_i. After the first pulse $\alpha(\epsilon_1)$, we obtain

$$I_{iz} \xrightarrow{\alpha(I_x\cos\epsilon_1 + I_y\sin\epsilon_1)} I_{iz}\cos\alpha + \frac{i}{2}[I_i^+\exp(-i\epsilon_1) - I_i^-\exp(i\epsilon_1)]\sin\alpha. \quad [3]$$

Because only the $+1$ quantum coherence will be selected out in the N-type MQF-COSY during t_1, we only consider the evolution of the I^+ term. Therefore, in the duration t_1, the evolution of the density operator is

$$\lambda(1)I_i^+ \xrightarrow{t_1} \lambda(1)I_i^+ \prod_{j'=1}^{q} I_{j'z}, \quad [4]$$

where $\lambda(1) = i/2 \sin\alpha \exp(-i\epsilon_1)$ and $j' \neq i$. On the right-hand side of Eq. [4], only the term $I_i^+ \prod_{j'=1}^{q} I_{j'z}$ that can be transformed into $+q$ quantum coherence is given. As noted above, rotations due to shift evolution and gradient effects are ignored. After the second RF pulse $\beta(\epsilon_2)$, we obtain the transformation

$$\lambda(1)I_i^+ \prod_{j'=1}^{q} I_{j'z} \xrightarrow{\beta(I_x\cos\epsilon_2 + I_y\sin\epsilon_2)} \lambda(1)\lambda(2)\prod_{i=1}^{q} I_i^+, \quad [5]$$

where $\lambda(2) = \{\cos^2\beta/2 \times ((i/2)\sin\beta)^{q-1}\exp[-i(q-1)\epsilon_2]\}$. In Eq. [5], only the $+q$ quantum coherence that survives the N-type MQF-COSY is given. Because the mixing delay and the second PFG pulse are used to select out the $+q$ quantum coherence, we can neglect the evolution in the mixing delay. After the third RF pulse $\gamma(\epsilon_3)$ and the third PFG, we obtain

$$\lambda(1)\lambda(2)\prod_{i=1}^{q} I_i^+ \xrightarrow{\gamma(\epsilon_3)} \xrightarrow{G_3} \lambda(1)\lambda(2)\lambda(3)\sum_i (I_i^- \prod_{j'} I_{j'z}), \quad [6]$$

where $\lambda(3) = \sin^2(\gamma/2)\exp(+i2\epsilon_3)(+i\sin\gamma)^{q-1}\exp[i(q-1)\epsilon_3]$. From Eq. [6] and the value of $\lambda(1)$, $\lambda(2)$, $\lambda(3)$, we obtain that the signal of N-type MQF-COSY (FID^N) is proportional to

TABLE 1
Coherence Transfer Pathway, Phase Error, and Amplitude of FID

Sequence	Type	Coherence pathway	Phase error and amplitude of FID signal
MQF-COSY	P	$0 \rightarrow -1 \rightarrow -q \rightarrow -1$	$\exp\{i[\epsilon_1 + (q-1)\epsilon_2 - (q-1)\epsilon_3]\}\sin\alpha\cos^2(\beta/2)(\sin\beta)^{q-1}\cos^2(\gamma/2)(\sin\gamma)^{q-1}$
	N	$0 \rightarrow +1 \rightarrow +q \rightarrow -1$	$\exp\{-i[\epsilon_1 + (q-1)\epsilon_2 - (q+1)\epsilon_3]\}\sin\alpha\cos^2(\beta/2)(\sin\beta)^{q-1}\sin^2(\gamma/2)(\sin\gamma)^{q-1}$
COSY	P	$0 \rightarrow -1 \rightarrow -1$	$\exp(i\epsilon_1)$ [a]
	N	$0 \rightarrow +1 \rightarrow -1$	$\exp[-i(\epsilon_1 - 2\epsilon_2)]$ [a]
MQC	P	$0 \rightarrow \pm 1 \rightarrow -q \rightarrow -1$	$\exp\{i[\pm\epsilon_1 + (q+1)\epsilon_2 - (q-1)\epsilon_3]\}\sin\alpha\cos^2(\gamma/2)(\sin\gamma)^{q-1}$ [b]
	N	$0 \rightarrow \pm 1 \rightarrow +q \rightarrow -1$	$\exp\{i[\pm\epsilon_1 - (q+1)\epsilon_2 + (q+1)\epsilon_3]\}\sin\alpha\sin^2(\gamma/2)(\sin\gamma)^{q-1}$ [b]
HMQC	P	$0 \rightarrow +1 \rightarrow 0 \rightarrow -2 \rightarrow -1$	$\exp[-i(\epsilon_1 - \epsilon_2 - 2\epsilon_3 + \epsilon_4)]\sin\alpha\sin\beta\sin\gamma$
	N	$0 \rightarrow +1 \rightarrow +2 \rightarrow 0 \rightarrow -1$	$\exp[-i(\epsilon_1 + \epsilon_2 - 2\epsilon_3 - \epsilon_4)]\sin\alpha\sin\beta\sin\gamma$
NOESY	P	$0 \rightarrow +1 \rightarrow -1 \rightarrow 0 \rightarrow +1 \rightarrow -1$	$\exp[i(\epsilon_1 - 2\epsilon_2 + \epsilon_3 - \epsilon_4 + 2\epsilon_5)]\sin\alpha\sin\beta\sin\gamma$
	N	$0 \rightarrow -1 \rightarrow +1 \rightarrow 0 \rightarrow +1 \rightarrow -1$	$\exp[i(-\epsilon_1 + 2\epsilon_2 - \epsilon_3 - \epsilon_4 + 2\epsilon_5)]\sin\alpha\sin\beta\sin\gamma$

[a] The dependency of the amplitude in COSY on RF pulses is given in Eqs. [14] and [15].
[b] In the MQC experiment, we use $\beta = 90°$ to retain the symmetrical pathways during Δ and use the maximum phase change of the second pulse between the symmetrical pathways.

$$\mathrm{FID}^{\mathrm{N}} \propto \sin\alpha\cos^2\frac{\beta}{2} \times (\sin\beta)^{q-1}\sin^2\frac{\gamma}{2}(+i\sin\gamma)^{q-1} \times \exp[-i\epsilon_1 - i(q-1)\epsilon_2 + i(q+1)\epsilon_3] \times \sum_i (I_i^- \prod_{j'} I_{j'z}). \quad [7]$$

Similarly, in P-type MQF-COSY ($\mathrm{FID}^{\mathrm{P}}$)

$$\mathrm{FID}^{\mathrm{P}} \propto \sin\alpha\cos^2\frac{\beta}{2} \times (\sin\beta)^{q-1}\cos^2\frac{\gamma}{2}(\sin\gamma)^{q-1} \times \exp[i\epsilon_1 + i(q-1)\epsilon_2 - i(q-1)\epsilon_3] \times \sum_i (I_i^- \prod_{j'} I_{j'z}). \quad [8]$$

In Eqs. [7] and [8], it can be seen clearly that the phase error in P-type MQF-COSY is smaller than that in N-type MQF-COSY, and the dependencies of the amplitudes on the rotation angles are different between P-type and N-type. The different phase errors will result in different t_1 noise levels, and the different amplitudes will rely on different optimized rotation angles. This is shown in the following.

Similarly, the FID signals of the absolute mode PFG COSY, MQC, HMQC, and NOESY are calculated, and the results are presented in Table 1. In Table 1, the FID signals contain only those terms that are related to the phase errors and the rotation angles of RF pulses.

B. t_1 Noise

The arbitrary phase error accumulated in the FID will result in t_1 noise in the 2D spectrum, after Fourier transform. Because the phase error ϵ_i has a small value, we can expand the exponential functions in the FID signals and keep only the first two terms. They are presented in Table 2. According to Parseval's theorem (*2*), the integrated noise power in the f_1 dimension of the final 2D spectrum will be the same as that in the t_1 time domain. Therefore the t_1 noise in an absolute value mode spectrum will be proportional to the square root of the sum of the squares of the error contributions. If the phase errors ϵ_1, ϵ_2, and ϵ_3 are all uncorrelated, and equal root mean square error signal amplitude ϵ, in the P-type and N-type PFG MQF-COSY, the ratios N/S of the root mean square error signal amplitudes to the moduli of the signals will be

$$(N/S)^{\mathrm{P}} = \sqrt{(\epsilon_1)^2 + [(q-1)\epsilon_2]^2 + [-(q-1)\epsilon_3]^2} = \epsilon\sqrt{1 + 2(q-1)^2} \quad [9]$$

and

$$(N/S)^{\mathrm{N}} = \sqrt{(-\epsilon_1)^2 + [-(q-1)\epsilon_2]^2 + [(q+1)\epsilon_3]^2} = \epsilon\sqrt{3 + 2q^2}; \quad [10]$$

therefore, the ratio of the t_1 noise in P-type pathway to that in N-type pathway MQF-COSY is

$$(N/S)^{\mathrm{P}}:(N/S)^{\mathrm{N}} = \sqrt{1 + 2(q-1)^2}:\sqrt{3 + 2q^2}. \quad [11]$$

In Eq. [11], when $q = 2$, namely in DQF-COSY, the ratio is $\sqrt{3}:\sqrt{11}$. When $q = 3$, in triple-quantum-filtered COSY, the ratio is $\sqrt{9}:\sqrt{21} = \sqrt{3}:\sqrt{7}$. The t_1 noise ratios of the absolute mode PFG COSY, MQF-COSY, MQC, HMQC, and NOESY are presented in Table 2. It can be seen in Table 2 that, in COSY, MQF-COSY, and MQC, the levels of t_1 noise in P-type experiments are lower than those in N-type experiments and

TABLE 2
t_1 Noise Level and the Ratio of t_1 Noise in P-Type to That in N-Type Experiments

			t_1 Noise relative to signal (N/S)		t_1 Noise relative to P-type	
Sequence	Type	Approximation of FID	Theory	Experiment	Theory	Experiment
MQF-COSY	P	$1 + i[\epsilon_1 + (q-1)\epsilon_2 - (q-1)\epsilon_3]$	$\sqrt{1+2(q-1)^2}\epsilon$	1/679[a]	1	1[a]
	N	$1 - i[\epsilon_1 + (q-1)\epsilon_2 - (q+1)\epsilon_3]$	$\sqrt{3+2q^2}\epsilon$	1/481[a]	$\sqrt{3+2q^2}/\sqrt{1+2(q-1)^2}$	1.41[a]
COSY	P	$1 + i\epsilon_1$	ϵ	1/1927[b]	1	1[b]
	N	$1 - i(\epsilon_1 - 2\epsilon_2)$	$\sqrt{5}\epsilon$	1/1318[b]	$\sqrt{5}$	1.74[b]
MQC	P	$1 + i[\pm\epsilon_1 + (q+1)\epsilon_2 - (q-1)\epsilon_3]$	$\sqrt{2+2q^2}\epsilon$	—	1	—
	N	$1 + i[\pm\epsilon_1 - (q+1)\epsilon_2 + (q+1)\epsilon_3]$	$\sqrt{1+2(q+1)^2}\epsilon$	—	$\sqrt{1+2(q+1)^2}/\sqrt{2+2q^2}$	—
HMQC	P	$1 - i(\epsilon_1 - \epsilon_2 - 2\epsilon_3 + \epsilon_4)$	$\sqrt{7}\epsilon$	—	1	—
	N	$1 - i(\epsilon_1 + \epsilon_2 - 2\epsilon_3 - \epsilon_4)$	$\sqrt{7}\epsilon$	—	1	—
NOESY	P	$1 + i(\epsilon_1 - 2\epsilon_2 + \epsilon_3 - \epsilon_4 + 2\epsilon_5)$	$\sqrt{11}\epsilon$	—	1	—
	N	$1 + i(-\epsilon_1 + 2\epsilon_2 - \epsilon_3 - \epsilon_4 + 2\epsilon_5)$	$\sqrt{11}\epsilon$	—	1	—

[a] The values of DQF-COSY experiments ($q = 2$).
[b] Ref. (*2*).

the ratio of t_1 noise in the P-type pathway to that in the N-type pathway is $\sqrt{1}:\sqrt{5}$ in COSY, $\sqrt{1+2(q-1)^2}:\sqrt{3+2q^2}$ in MQF-COSY, and $\sqrt{2+2q^2}:\sqrt{1+2(q+1)^2}$ in MQC, while the levels of the t_1 noise in P-type are equal to those in N-type in the absolute value mode PFG HMQC and NOESY.

C. Optimized RF Pulse Rotation Angles

The dependencies of the signal amplitudes on the RF pulse angles are presented in Table 3. In each pulse sequence, there are optimized RF pulse angles at which the maximum value of signal amplitude will occur. In the absolute value mode PFG MQF-COSY ($q \geq 2$), from Eqs. [7] and [8] and Table 3, we find that the maximum value of the signal amplitude occurs at

$$\alpha = \pi/2$$

$$\beta = 2 \text{ arc cot}\sqrt{\frac{2}{q-1}+1}, \quad \text{for } q \geq 2$$

$$\gamma = \begin{cases} 2 \text{ arc cot}\sqrt{\dfrac{2}{q-1}+1}, & \text{for } q \geq 2, \\ & \text{P-type MQF-COSY} \\ \pi - 2 \text{ arc cot}\sqrt{\dfrac{2}{q-1}+1}, & \text{for } q \geq 2, \\ & \text{N-type MQF-COSY} \end{cases} \quad [12]$$

where α, β, and γ are the rotation angles of the three RF pulses in the MQF-COSY sequence, shown in Fig. 1. In the MQF-COSY sequence, the ratio of signal intensity in an experiment with the optimized angles to that in an experiment with α, β, $\gamma = 90°$ is

TABLE 3
Amplitude of the FID Signal and the Optimized RF Pulse Angle

Sequence	Type	Amplitude of FID	Optimized RF pulse angles
MQF-COSY	P	$\sin\alpha\cos^2(\beta/2)(\sin\beta)^{q-1}\cos^2(\gamma/2)(\sin\gamma)^{q-1}$	$\alpha = 90°$, $\beta, \gamma = 2 \text{ arc cot}\sqrt{2/(q-1)+1}$, for $q \geq 2$
	N	$\sin\alpha\cos^2(\beta/2)(\sin\beta)^{q-1}\sin^2(\gamma/2)(\sin\gamma)^{q-1}$	$\alpha = 90°$, $\beta = 2 \text{ arc cot}\sqrt{2/(q-1)+1}, \gamma = 180° - \beta$, for $q \geq 2$
DQF-COSY	P	$\sin\alpha\cos^2(\beta/2)\sin\beta\cos^2(\gamma/2)\sin\gamma$	$\alpha = 90°$, $\beta, \gamma = 60°$
	N	$\sin\alpha\cos^2(\beta/2)\sin\beta\sin^2(\gamma/2)\sin\gamma$	$\alpha = 90°$, $\beta = 60°$, $\gamma = 120°$
MQC	P	$\sin\alpha\cos^2(\gamma/2)(\sin\gamma)^{q-1}$	$\alpha = 90°$, $\gamma = 2 \text{ arc cot}\sqrt{2/(q-1)+1}$, for $q \geq 2$[a]
	N	$\sin\alpha\sin^2(\gamma/2)(\sin\gamma)^{q-1}$	$\alpha = 90°$, $\gamma = 180° - 2 \text{ arc cot}\sqrt{2/(q-1)+1}$, for $q \geq 2$[a]
HMQC	P	$\sin\alpha\sin\beta\sin\gamma$	$\alpha, \beta, \gamma = 90°$
	N	$\sin\alpha\sin\beta\sin\gamma$	$\alpha, \beta, \gamma = 90°$
NOESY	P	$\sin\alpha\sin\beta\sin\gamma$	$\alpha, \beta, \gamma = 90°$
	N	$\sin\alpha\sin\beta\sin\gamma$	$\alpha, \beta, \gamma = 90°$

[a] In MQC experiment, $\beta = 90°$ is used to retain the symmetrical pathways during Δ.

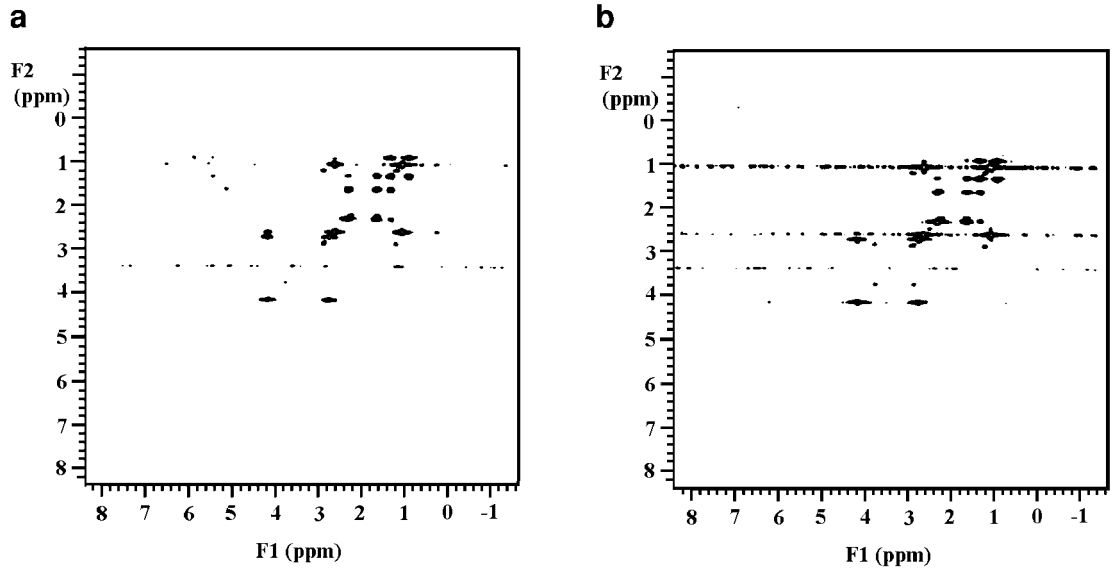

FIG. 2. Absolute value mode proton PFG DQF-COSY spectra. (a) P-type and (b) N-type versions of the pulse sequence in Fig. 1.

$$S_{\text{opt}}/S_{90^\circ} = 4\left[\cos^2\left(\text{arc cot}\sqrt{\frac{2}{q-1}+1}\right)\times \sin^{q-1}\left(2\ \text{arc cot}\sqrt{\frac{2}{q-1}+1}\right)\right]^2. \quad [13]$$

When $q = 2$, the MQF-COSY is the conventional DQF-COSY, in which the optimized angles are $\alpha = 90°$, $\beta = 60°$, and $\gamma = 60°$ (P-type) or $\alpha = 90°$, $\beta = 60°$, and $\gamma = 120°$ (N-type). About a 69% increase in signal intensity may be achieved by using the optimized RF pulse angles. When $q = 3$, in the triple-quantum-filtered COSY experiment, the optimized angles are $\alpha = 90°$, $\beta = 70.5°$, and $\gamma = 70.5°$ (P-type) or $\alpha = 90°$, $\beta = 70.5°$, and $\gamma = 109.5°$ (N-type). The increases in sensitivities of N-type and P-type are about 40% over those of the same experiments using $\alpha, \beta, \gamma = 90°$.

In the N-type absolute value mode PFG COSY experiment, the diagonal peak comes from

$$I_{iz} \xrightarrow{\alpha(\epsilon_1)} \frac{i}{2} I_i^+ \sin\alpha \exp(-i\epsilon_1) \xrightarrow{t_1}$$

$$\frac{i}{2}\sin\alpha(I_i^+\cos\pi Jt_1 - i2I_i^+I_{jz}\sin\pi Jt_1) \times \exp(-i\epsilon_1) \xrightarrow{\beta(\epsilon_2)} \frac{i}{2}\sin\alpha \times \left(I_i^-\sin^2\frac{\beta}{2}\cos\pi Jt_1 - i2I_i^-\sin^2\frac{\beta}{2}I_{jz}\cos\beta\sin\pi Jt_1\right) \times \exp(-i\epsilon_1 + i2\epsilon_2), \quad [14]$$

where the spins I_i and I_j are the operators of a two-spin weak coupled system. The cross peak comes from

$$I_{iz} \xrightarrow{\alpha(\epsilon_1)} \frac{i}{2} I_i^+ \sin\alpha \exp(-i\epsilon_1) \xrightarrow{t_1}$$

$$-\sin\alpha I_i^+ I_{jz}\sin\pi Jt_1\exp(-i\epsilon_1) \xrightarrow{\beta(\epsilon_2)} -\frac{1}{2}\sin\alpha \times I_{iz}\sin\beta \times I_j^-\sin\beta\sin\pi Jt_1\exp(-i\epsilon_1 + i2\epsilon_2). \quad [15]$$

From Eqs. [14] and [15], we can conclude that in N-type COSY the diagonal peaks will be deemphasized when $\alpha = 90°$ and $\beta < 90°$, while emphasized when $\alpha = 90°$ and $\beta > 90°$. Similarly, in P-type COSY, when $\alpha = 90°$ and $\beta < 90°$, the diagonal peaks will be emphasized, while $\alpha = 90°$ and $\beta > 90°$ will be deemphasized.

In the MQC experiment, the symmetrical pathways are retained by using $\beta = 90°$. The optimized angles are

$$\alpha = \pi/2$$

$$\gamma = \begin{cases} 2\ \text{arc cot}\sqrt{\dfrac{2}{q-1}+1}, & \text{for } q \geq 2, \text{ P-type MQC} \\ \pi - 2\ \text{arc cot}\sqrt{\dfrac{2}{q-1}+1}, & \text{for } q \geq 2, \text{ N-type MQC} \end{cases}. \quad [16]$$

In the MQC sequence, the ratio of intensity in the experiment with the optimized angles to that in the experiment with α, β, $\gamma = 90°$ is

$$S_{opt}/S_{90°} = 2\left[\cos^2\left(\text{arc cot}\sqrt{\frac{2}{q-1}+1}\right) \times \sin^{q-1}\left(2\ \text{arc cot}\sqrt{\frac{2}{q-1}+1}\right)\right]. \quad [17]$$

However, in HMQC and NOESY experiments, all of the optimized RF pulse rotation angles are equal to 90 or 180°.

III. EXPERIMENTS AND RESULTS

All of the proton absolute value experiments were acquired on a Varian Unity 500 spectrometer, using a 5-mm triple-resonance pulsed field gradient probe. The sample used is (*N*,*N*-diethylamino)ethyl caproate in deuterochloroform.

Figure 2 shows the absolute mode PFG DQF-COSY spectra. The spectral width was set to 5000 Hz in each dimension, with 2048 complex data points in t_2 (acquisition time 0.205 s) and 256 t_1 increments. The recycle time was 9.6 s. The PFG DQF-COSY were carried out using four scans per increment with rectangular gradient pulses of 5-ms duration and approximately 8 G cm^{-1} for G_1 strength (G_1:G_2:G_3 = 1:1:±3). The absolute value spectra were obtained by one-time zero-filling in t_1 and sine-bell weighting centered on 0.102 s in t_1 and 0.022 s in t_2, respectively. We use the region between 6 and 7 ppm in the absolute value f_1 cross section through f_2 = 2.28 ppm for the t_1 noise samples. The ratios of the t_1 noise are presented in Table 2. From Fig. 2 and Table 2, we can see clearly that the level of the t_1 noise in P-type MQF-COSY is lower than that in N-type.

Figure 3 shows the 1D spectra of the f_2 dimension (directly detected dimension) of the absolute value mode PFG DQF-COSY and TQF-COSY (triple-quantum-filtered COSY). All of the spectra in Fig. 3 were recorded with only one transient and only one t_1 increment, t_1 = 20 ms. The peak amplitudes are numbered above the peaks. From Fig. 3, we note that the peak heights of P-type are lower than those of N-type, because the N-type pathway can refocus the field inhomogeneity. The sensitivity enhancements are clearly seen in Fig. 3.

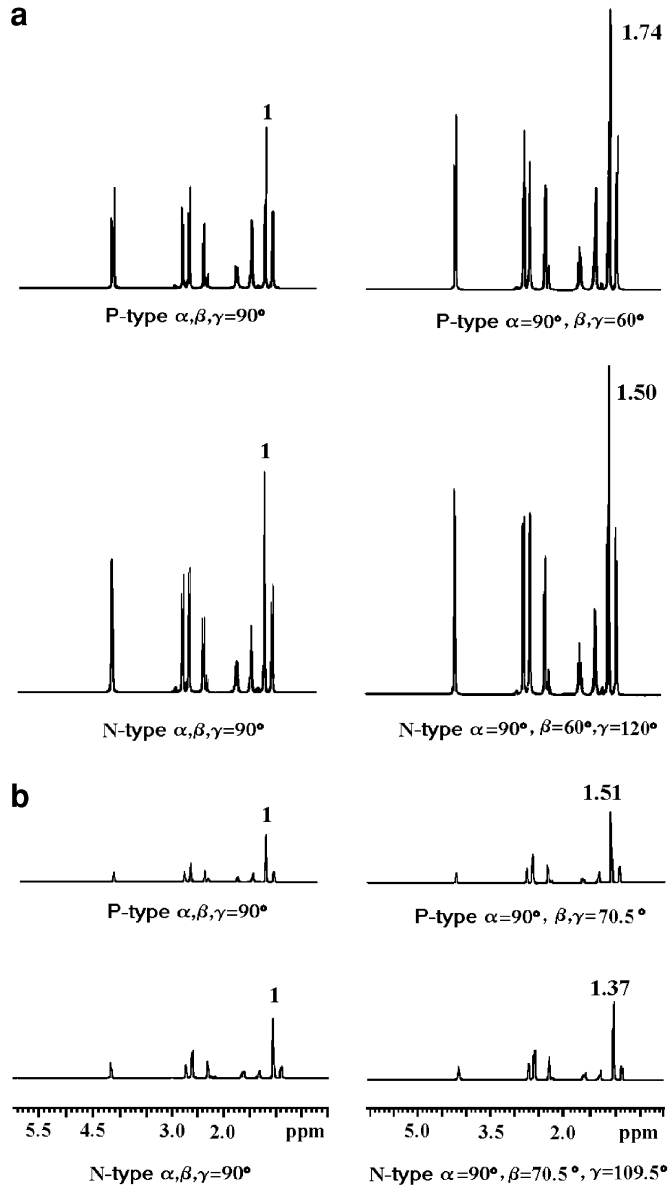

FIG. 3. Absolute value mode PFG MQF-COSY spectra of (a) double-quantum-filtered COSY (DQF-COSY) and (b) triple-quantum-filtered COSY (TQF-COSY) using the pulse sequence shown in Fig. 1. The numbers above the peaks are the peak intensities relative to the same experiments using α, β, $\gamma = 90°$.

IV. DISCUSSION

As the foregoing analysis and experiments show, the t_1 noise and signal amplitude are closely related to the coherence transfer pathway and the RF pulses of the experiment. Our theoretical results indicate that t_1 noise in P-type COSY, MQF-COSY, and MQC experiments is lower than those in N-type experiments. The theoretical ratios of t_1 noise in P-type to that in N-type is 1:$\sqrt{5}$ in COSY, $\sqrt{1+2(q-1)^2}$:$\sqrt{3+2q^2}$ in MQF-COSY (when q = 2, in DQF-COSY, the ratio is $\sqrt{3}$:$\sqrt{11}$ ≈ 1:1.91), and $\sqrt{2+2q^2}$:$\sqrt{1+2(q+1)^2}$ in MQC, while in HMQC and NOESY both ratios are 1:1. In our experiments, the ratio in P-type DQF-COSY to that in N-type is 1:1.41. It is reasonable that our experiment ratio is lower than the theoretical value because there are other sources of t_1 noise, such as frequency, gain, or shimming irreproducibility, but most of these sources do not produce a different t_1 noise effect between the P-type pathway and the N-type pathway. The t_1 noise also shows a dependence on the time-domain weighting functions used; however, the t_1 noise advantages of

P-type over N-type experiments remain clear over a wide range of different processing conditions. Our result for COSY experiments is similar to that obtained by Horne and Morris (*2*), but our calculation method is different. The results presented here may be significant in situations such as *in vivo* spectroscopy. The t_1 noise rather than thermal noise may be the limiting factor in the detection of cross peaks where signals are sufficiently strong. On a modern NMR instrument this may not be until the signal-to-thermal-noise ratio is over 1000:1, but in biological applications the P-type experiment may have advantages over the N-type because of the spectroscopy instabilities (*2*). The differences of t_1 noise in pulse sequences stem from the phase errors being different in different coherence pathways. For example, the phase error is $\exp(+i2\epsilon)$ in $I^+ \rightarrow I^-$, while zero in $I^- \rightarrow I^-$.

The optimized RF pulse angles may result in sensitivity enhancement in the experiments. It arises from this that the maximal conversion efficiency of coherence occurs at the optimized angles, which are not always the 90° pulses. Our optimized angles in MQF-COSY show an increase in sensitivity of about $4(\cos^2\theta \sin^{q-1}2\theta)^2 - 1$ (θ = arc cot $\sqrt{2/(q-1)+1}$) over the same experiment using 90° pulses. In MQC, the increase of sensitivity is $2\cos^2\theta \sin^{q-1}2\theta - 1$ θ = arc cot $\sqrt{2/(q-1)+1}$). If a phase-sensitive spectrum is acquired by recording N-type and P-type signals, respectively, the sensitivity in N-type being higher than that in P-type will result in a spectrum with a phase-twist lineshape, because adding the anti-reversed N-type and P-type spectra together cannot cancel the dispersive parts of the phase twist. Therefore, choosing a set of suitable rotation angles of RF pulses or using suitable weighting coefficients in Fourier transform to make sensitivity in the N-type equal to that in the P-type is important in performing phase-sensitive experiments.

ACKNOWLEDGMENTS

This work has been supported by the Natural Science Foundation of Fujian Province, People's Republic of China, and by the State Key Laboratory for Physical Chemistry of the Solid Surface.

REFERENCES

1. J. Cavanagh and M. Rance, Sensitivity improvement in isotropic mixing (TOCSY) experiments, *J. Magn. Reson.* **88,** 72–85 (1990).
2. T. J. Horne and G. A. Morris, P-type gradient-enhanced COSY experiments show lower t_1 noise than N-type, *Magn. Reson. Chem.* **35,** 680–686 (1997).
3. G. X. Lin, X. L. Liao, D. H. Lin, S. K. Zheng, Z. Chen, and Q. Y. Wu, P-type PFG DQF-COSY experiments show lower t_1 noise level than N-type, *Chin. J. Magn. Reson.* **16,** 11–18 (1999).
4. T. H. Mareci and R. Freeman, Echoes and antiechoes in coherence transfer NMR: Determining the signs of double-quantum frequencies, *J. Magn. Reson.* **48,** 158–163 (1982).
5. J. F. Shen and P. S. Allen, Enhancement of double-quantum-filtered signals using optimized tip angle RF pulses, *J. Magn. Reson.* **90,** 606–611 (1990).
6. O. W. Sorensen, G. W. Eich, M. H. Levitt, G. Bodenhausen, and R. R. Ernst, Product operator formalism for the description of NMR pulse experiments, *Prog. Nucl. Magn. Reson. Spectrosc.* **16,** 163–192 (1983).
7. T. Parella, Pulsed field gradients: A new tool for routine NMR, *Magn. Reson. Chem.* **36,** 467–495 (1998).
8. R. E. Hurd, Gradient-enhanced spectroscopy, *J. Magn. Reson.* **87,** 422–428 (1990).